

RESEARCH ARTICLE

10.1002/2015JA021985

Key Points:

- Tail reconnection at Saturn organized by northern/southern phase
- Events linked to current sheet thinning and outward displacement of field and plasma
- Little evidence for visibility effects associated with north-south motions of the plasma sheet

Correspondence to:

C. M. Jackman,
c.jackman@soton.ac.uk

Citation:

Jackman, C. M., G. Provan, and S. W. H. Cowley (2016), Reconnection events in Saturn's magnetotail: Dependence of plasmoid occurrence on planetary period oscillation phase, *J. Geophys. Res. Space Physics*, 121, 2922–2934, doi:10.1002/2015JA021985.

Received 3 OCT 2015

Accepted 2 FEB 2016

Accepted article online 5 FEB 2016

Published online 6 APR 2016

Reconnection events in Saturn's magnetotail: Dependence of plasmoid occurrence on planetary period oscillation phase

C. M. Jackman¹, G. Provan², and S. W. H. Cowley²

¹School of Physics and Astronomy, University of Southampton, Southampton, UK, ²Department of Physics and Astronomy, University of Leicester, Leicester, UK

Abstract During its exploration of Saturn's magnetotail the Cassini magnetometer has detected many in situ examples of magnetic reconnection, in the form of plasmoids, traveling compression regions (TCRs), and dipolarizations. Meanwhile, many magnetospheric phenomena have been shown to be organized with particular regularity by planetary period oscillation systems driven separately from the Northern and Southern Hemispheres of the planet. Here we examine the relationship between the occurrence of plasmoids and TCRs and the magnetic phases of the northern and southern systems. We find a striking degree of organization of the events by both northern and southern phases, with events linked preferentially to intervals in which the magnetospheric plasma and field lines are displaced outward from the planet and the current sheet thinned, both effects being likely to favor the occurrence of reconnection and plasmoid-related mass loss. Little evidence is found for significant visibility effects associated with north-south motions of the plasma sheet.

1. Introduction

Since the arrival of the Cassini spacecraft at Saturn in 2004 it has been possible to examine kronian magnetospheric dynamics through a mix of local in situ measurements (magnetic fields and plasma) as well as via remote sensing of the radio emissions and planetary aurora. The best chance to observe dynamics in the magnetotail in situ came in 2006 when the spacecraft executed its deepest tail orbits, out to $68 R_S$ ($1 R_S = 60268$ km). Many papers have been published examining the local properties of reconnection events, which fall into three broad categories: plasmoids, traveling compression regions (TCRs), and dipolarizations. Plasmoids represent lumps of plasma and magnetic field broken off the plasma sheet via reconnection which propagate downtail [e.g., Jackman *et al.*, 2007, 2008, 2011, 2014; Hill *et al.*, 2008], while TCRs are the signatures of the warping of the lobe magnetic field lines by plasmoids passing in the nearby plasma sheet [e.g., Slavin *et al.*, 1984]. Finally, dipolarization of the field planetward of the X line has also been reported on several occasions at Saturn [e.g., Bunce *et al.*, 2005; Russell *et al.*, 2008; Thomsen *et al.*, 2013; Jackman *et al.*, 2013, 2015].

As the study of tail reconnection has advanced and the catalogs of events have built up, attempts have been made to place the reconnection events in the context of global magnetospheric dynamics, and in particular to examine possible links between reconnection and the "planetary period oscillations" (PPOs) that are ubiquitous in Saturn magnetosphere-related data sets (see, e.g., review by Carbary and Mitchell [2013] and references therein). Initial suggestions that plasmoids are observed every planetary rotation [Burch *et al.*, 2008] have been shown to be incorrect if the appropriate coordinate system is used to examine the tail field [Jackman *et al.*, 2009a]. The important distinction must be made between regular wavy motion of Saturn's current sheet and the dramatic changes in field morphology related to reconnection.

Kurth *et al.* [2008] devised the SLS3 system for organizing the periodicity observed in Saturn Kilometric Radiation (SKR), specifically in that case for the then-dominant southern planetary period oscillation (PPO) system. This phase system is an updated version of the original SLS system devised from the modulation of SKR as seen in Voyager data and the subsequent SLS2 system which was valid for the southern modulations over the first two years of the Cassini mission. Jackman *et al.* [2009b] examined the timings of nine reconnection events from 2006 against this SLS3 system and found that eight out of nine events occurred in a particular sector of SKR phase, where the SKR power was rising with time. This implied that although reconnection events are not seen at the same time every planetary rotation, there did appear to be a preferential longitude for mass release.

Since the publication of that work, the study of PPOs has advanced enormously, with the separation of the northern and southern magnetic and radio periods and the development of phase models based on both

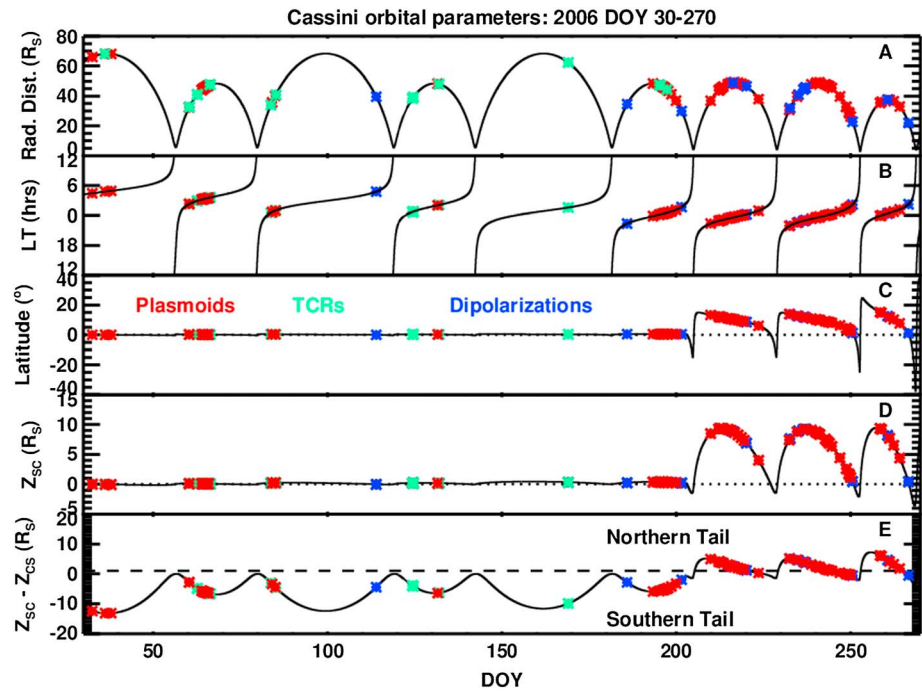


Figure 1. (a) Radial distance, (b) local time, (c) latitude, and (d) displacement from Saturn’s equator Z_{SC} positive northward for Cassini from day 30 to 270 of 2006. Asterisks show the timing of 99 reconnection events from the Jackman *et al.* [2014] catalog with red for plasmoids, green for TCRs, and blue for dipolarizations. (e) The spacecraft position relative to the modeled Arridge *et al.* [2008] current sheet for a hinge position of $29 R_S$, where negative values mean that the spacecraft was southward of the modeled current sheet position. A horizontal dashed line is placed at $Z_{SC} - Z_{CS} = 1 R_S$, representing the mean center of the current sheet for this interval as determined by Provan *et al.* [2012] (see their Figure 10b).

data sets [Gurnett *et al.*, 2009, 2011; Andrews *et al.*, 2008, 2010, 2012; Provan *et al.*, 2009, 2011; Lamy, 2011]. In this work we seek to further explore the link between tail reconnection events at Saturn and the PPO phases, since the latter effects are known to modulate the radial distribution of plasma within the magnetosphere [Burch *et al.*, 2009], the thickness of the plasma sheet in the tail [Provan *et al.*, 2012], as well as its north-south position about the seasonally varying average [Arridge *et al.*, 2008, 2011; Provan *et al.*, 2012]. The first two of these effects are likely players in influencing the stability of the tail current sheet to reconnection, while the third may also influence the visibility of the events. We aim to explore the statistical significance of any correlations and to understand if these correlations correspond to a genuine increased likelihood of occurrence or to visibility effects. In section 2 we introduce the data set and methodology, in section 3 we present our results, and in section 4 we summarize.

2. Data Set

Figure 1 shows the progression of the Cassini orbit from day 30–270 of 2006, the interval which encompasses the 99 reconnection events from the Jackman *et al.* [2014] (hereafter J14) list. This list is comprised of 69 plasmoids (red asterisks) observed tailward of the reconnection site, 17 TCRs (green asterisks), and 13 dipolarizations (blue asterisks) observed planetward of the reconnection site. Events were originally identified by J14 as bipolar changes in the north-south component of the magnetic field, using data from the Cassini magnetometer instrument [Dougherty *et al.*, 2004]. TCRs generally display smaller north-south perturbations than plasmoids or dipolarizations but are recognized by the smooth compression of the total magnetic field, associated with the draping of the lobe field lines around the bulging plasma sheet beneath. The events are seen at radial distances (Figure 1a) from 22 to $68 R_S$, with plasmoids (tailward of the reconnection site) over the range ~ 26 to $68 R_S$ and dipolarizations (planetward of the reconnection site) over the range ~ 22 to $49 R_S$. This spread illustrates that the X line is highly mobile within the observed region, perhaps influenced by external solar wind conditions (e.g., as modeled by Jia *et al.* [2012]). The local time (Figure 1b) spread of events is from ~ 21 to 04 h, with 34 events premidnight and 65 events postmidnight, with this dawn-dusk split

primarily a function of the relative amount of time spent by the spacecraft in these regions (although with a slight preference for mass release toward dawn).

The spacecraft latitude (Figure 1c) illustrates the two different types of orbit in 2006. The first type of orbit (Revs 20 outbound to 26 inbound) is seen up to ~day 205 when the spacecraft spends most of its time close to the equatorial plane. Given the Southern Hemisphere summer conditions in 2006, we may expect that this means that Cassini spends most of its time in the southern lobe, beneath the hinged current sheet [Arridge *et al.*, 2008; Jackman and Arridge, 2011]. During this time, the spacecraft observed 28 (out of 69) plasmoids, 17 (out of 17) TCRs, and 3 (out of 13) dipolarizations, at latitudes between -0.04 and $+0.45^\circ$. The large number of TCRs is indicative of the time spent in the lobe, far from the central current sheet where plasmoids are formed and propagate. We may infer that this interval may contain the largest events seen further from the center of the current sheet. The second type of orbit (Revs 26 outbound to 29 inbound) is seen after day 205 when the spacecraft executes higher-latitude excursions, spending more time near the center of the current sheet and some time in the northern lobe. During this time, the spacecraft observed 41 (out of 69) plasmoids, 0 TCRs, and 10 (out of 13) dipolarizations at latitudes between $+0.38$ and $+15.2^\circ$, at an overall higher temporal rate than on the near-equatorial orbits. We expect that the lack of TCRs during this interval is linked to the spacecraft's position relatively close to the hinged current sheet. We thus infer that this later, higher-latitude interval may contain many smaller events.

As stated above, Saturn's current sheet is observed to be hinged upward out of Saturn's equatorial plane due to seasonal effects. This hinging was modeled by Arridge *et al.* [2008] who noted that during Southern Hemisphere summer conditions (such as those in 2006), the solar wind attack angle was such that it would cause an asymmetric lift of the current sheet into a bowl shape northward of the equator. The formula which governs the current sheet position is given by equation (1), which we have used to estimate the current sheet position at the times of the observed reconnection events. The mean location of the current sheet northward of Saturn's equatorial plane, z_{CS} , is given by

$$z_{CS} = \left[\rho - r_H \tanh\left(\frac{\rho}{r_H}\right) \right] \tan\theta_{SUN}, \quad (1)$$

where r_H is the hinging distance (taken to be $29 R_S$ as in Arridge *et al.* [2008]), θ_{SUN} is the latitude of the Sun, and ρ is the cylindrical radial distance. This expression describes the deformation of the current sheet out of the equatorial plane into a bowl shape, symmetrical in local time.

Figure 1d shows the displacement z_{SC} of the spacecraft relative to the equatorial plane over the interval, positive northward, while Figure 1e shows the difference between this position and the modeled current sheet position given by equation (1). While the Arridge *et al.* [2008] model provides a good first approximation to the position of the current sheet, Provan *et al.* [2012] found for this specific data set that the mean position of the tail current sheet center was displaced by $\sim 1 R_S$ northward from that given by the formula (see their Figure 10b), shown by the dashed horizontal line in Figure 1e. This figure clearly illustrates that the events earlier in the interval are mostly observed well southward of the current sheet center, while those later in the year are typically located closer to the center and both northward and southward of the mean current sheet position.

2.1. Magnetic Phase Model

As indicated in section 1, the Cassini spacecraft's suite of instruments has observed a range of oscillations close to the planetary rotation period since Saturn orbit insertion in 2004. The properties of the planetary period magnetic field oscillations have been studied in depth [e.g., Cowley *et al.*, 2006; Giampieri *et al.*, 2006; Provan *et al.*, 2009, 2011, 2012; Andrews *et al.*, 2010, 2011, 2012], consisting of two components which correspond to the northern and southern SKR periodic modulations [Gurnett *et al.*, 2009, 2011; Lamy, 2011], having periods ~ 10.6 and ~ 10.8 h, respectively, during the interval studied here. These two magnetic oscillations are combined together within the inner quasi-dipolar "core" region of the magnetosphere (dipole $L \leq 12$), giving rise to "beat" modulations in the phase and amplitude of the observed oscillations, from which the individual northern and southern phases, periods, and amplitudes have been determined [Provan *et al.*, 2011; Andrews *et al.*, 2012].

In brief, Andrews *et al.* [2012] outlined the principles which allow the determination of both northern and southern phases, $\Phi_n(t)$ and $\Phi_s(t)$, independently from the empirical magnetic phase data, provided that both

oscillations are of sufficient amplitude. These phases define the orientation relative to the Sun of the perturbation magnetic fields of the northern and southern PPO systems at any instant (illustrated in detail in Figure 1 of Provan *et al.* [2012]). Specifically, the phase angles give the azimuth relative to noon in which the quasi-uniform equatorial perturbation field points radially outward from Saturn at any time, i.e., the azimuth at which the equatorial radial field B_r has its maximum.

Andrews *et al.* [2012] showed that during the preequinox interval studied here the oscillation periods determined for the northern and southern magnetic systems generally agree very well with the corresponding northern and southern modulation periods determined from the SKR data by Lamy [2011] and Gurnett *et al.* [2011], typically within ~ 10 s. The northern quasi-uniform equatorial field points close to sunward (0° azimuth) at the times of northern SKR maxima, thus $\Phi_{\text{nMAG}} - \Phi_{\text{nSKR}} \approx 0^\circ$ (modulo 360°), while the southern quasi-uniform equatorial field points close to tailward (180° azimuth) at the times of southern SKR maxima, thus $\Phi_{\text{sMAG}} - \Phi_{\text{sSKR}} \approx 180^\circ$ (modulo 360°). However, for the specific interval examined here the northern magnetic signal proved hard to discern within the core magnetic field data such that its phase is unreliable, in which case, in view of the above result ($\Phi_{\text{nMAG}} - \Phi_{\text{nSKR}} \approx 0^\circ$ modulo 360°), we use the northern SKR phase of Lamy [2011] as a direct proxy for the northern magnetic phase in this work.

While the northern and southern system perturbations are observed individually over the two polar regions and in the lobes of the magnetic tail [Andrews *et al.*, 2012; Provan *et al.*, 2012; Hunt *et al.*, 2015], as indicated above, combined oscillations are observed in the quasi-dipolar region and extended plasma sheet. The perturbations which occur at a given point at time t depend on the position-dependent phase

$$\Psi_{\text{N,S}}(\phi, t) = \Phi_{\text{N,S}}(t) - \phi, \quad (2)$$

where ϕ is the azimuth at the observation point (spacecraft) measured from noon, positive in the sense of planetary rotation (such that, e.g., $\phi = 90^\circ$ at dusk). These phases define the instantaneous position of the observer relative to the rotating PPO current systems and hence the perturbation fields at the point of observation. Thus, for example, the quasi-uniform field points radially outward at the observation point when $\Psi_{\text{N,S}}(\phi, t) \approx 0^\circ$, corresponding to $\Phi_{\text{N,S}}(t) \approx \phi$. For application to field perturbations in the plasma sheet two further “corrections” are also employed, however, as discussed in the following section. The implication of the perturbations for the structure of the tail plasma sheet and the formation of plasmoids will be discussed in section 3.1.

2.2. Tracking to Inferred Reconnection Site and Radial Phase Delay

We first note that the times of the events in the J14 catalog are the times at which field deflections were observed at the spacecraft, and not the times at which the reconnection events themselves released plasmoids. As our aim is to associate the times of reconnection events with the phase of magnetospheric periodicities, it is more appropriate to employ the phases at the times of the reconnection events themselves, a point previously recognized by Jackman *et al.* [2009b]. Given the relative lack of published plasma data or information about the X line position at the time of that study, they took the simplistic approach to “track” plasmoid observations back to an inferred reconnection site at $30 R_S$ given a propagation speed of 800 km s^{-1} (based on a single in situ plasma velocity measurement by Hill *et al.* [2008]). We are now in a better position to conduct such tracking in a more physically realistic manner.

We might reasonably assume, e.g., from the data in Figure 1a, that the magnetotail reconnection X line lies typically at least $25 R_S$ from the planet on average. This assumption is also supported by observations of energetic neutral atom (ENA) emissions by Mitchell *et al.* [2005] which place the X line in the region of $20\text{--}30 R_S$, MHD modeling by Jia *et al.* [2012] which places the X line in the region of $25\text{--}40 R_S$, and a single direct observation of the diffusion region by Arridge *et al.* [2015] which places it at $36 R_S$. For a given observation of a tailward moving plasmoid or associated TCR at a distance R_{OBS} , we may then say that the reconnection site lies at some fraction, f , of the radial distance of the spacecraft from this minimum X line location, $R_0 = 25 R_S$. We thus take $R_{\text{RCN}} = R_0 + f(R_{\text{OBS}} - R_0)$ for some f in the range $0 \leq f \leq 1$. The distance from the spacecraft to the reconnection site is then $(1 - f)(R_{\text{OBS}} - R_0)$, such that the time of a reconnection event T_{RCN} that was observed at Cassini at T_{OBS} is

$$T_{\text{RCN}} = T_{\text{OBS}} - (1 - f)(R_{\text{OBS}} - R_0)/V_p \quad (3)$$

where V_p is the speed of propagation of the plasmoid (or TCR), assumed to be approximately radial. We take

this speed to be 300 km s^{-1} on average based on the mean of a set of 35 in situ measurements of plasmoid speeds made by the CAPS instrument during 2006 and presented by J14. On the basis of the broadly spread nature of the events in Figure 1a we then simply take the value of f to be 0.5, such that in the absence of direct evidence we assume that the plasmoid was not formed at the minimum radial distance, nor at the spacecraft, but typically half way between. The range of R_{RCN} values for the 65 “grouped” plasmoids and TCRs in this study (see below) is found to be 25.6 to $46.6 R_S$ (see Table A1), with a mean value of $34.5 R_S$. The corresponding mean value of $(R_{\text{OBS}} - R_0)$ is $\sim 19 R_S$. We may estimate a reasonable uncertainty range in T_{RCN} by taking f to vary between, say, 0.25 and 0.75, such that $\delta T_{\text{RCN}} \approx \pm 0.25(R_{\text{OBS}} - R_0)/V_P$. Using the mean value of $(R_{\text{OBS}} - R_0)$ and the above value of V_P , we thus estimate that typically $\delta T_{\text{RCN}} \approx \pm 15 \text{ min}$, corresponding to $\sim \pm 2.5\%$ of a PPO rotation or $\sim \pm 10^\circ$ in PPO phase. The uncertainty in PPO phase associated with the uncertainty in the radial distance of reconnection onset is thus not expected to be large.

We also note that the above radial range for reconnection onset, $\sim 26\text{--}47 R_S$, lies well outside of the core magnetosphere region for which the magnetic phase systems were originally defined (dipole $L \leq 12$). At these larger radial distances we must also include a radial propagation phase delay of $\sim 3 R_S^{-1}$, based on the results of *Arridge et al.* [2011] and *Provan et al.* [2012], which is subtracted from the phase based on equation (2). These phase adjustments are considerably more important than those associated with radial propagation discussed above, lying in the range $\sim 40^\circ\text{--}100^\circ$, with a mean value of $\sim 70^\circ$. We also employ the azimuth ϕ of the spacecraft in equation (2), again on the assumption that the propagation of the observed event perturbations was to a first approximation radial.

One other factor which needs to be taken into account when analyzing the statistical relationship between such events and magnetospheric periodicities is the grouping of the events. Care must be taken not to skew the statistics through the inclusion of multiple events in quick succession which would unnaturally weight the occurrence. In J14, events were split into categories referred to as “isolated,” “paired,” or “multiple” depending on whether other events were observed in close proximity, in that case within 180 min. Paired or multiple events were considered to be associated with the same reconnection episode. Thus, for the purposes of the present work, such events are grouped together and only the timing of the first event in the pair/series is considered when comparing with the PPO phases. This reduces the data set from the 99 examples shown in Figure 1 to 77 events. Furthermore, due to the event tracking to the inferred reconnection site, it is inappropriate to include dipolarizations in the data set, because we have less information about their propagation speed away from the reconnection site. Thus, we focus solely on plasmoids and TCRs tailward of the X line, which reduces the data set from 77 to 65 grouped events, the properties of which are listed in Table A1.

3. Results

3.1. PPO Perturbations of the Tail Current Sheet

We now discuss the effect of PPO-related perturbations on the tail current sheet, and possible consequences for the occurrence of reconnection and plasmoid visibility, based largely on the previous results of *Arridge et al.* [2011] and *Provan et al.* [2012]. When the equatorial radial perturbation field Br is positive at the local time of observation, with maximum values at $\Psi_{\text{N,S}} \approx 0^\circ$ (modulo 360°) for both systems, such that it points in the same direction as the field in the north lobe but opposite to the field in the south lobe, then the current sheet is displaced to the south. Similarly, when Br is negative at the local time of observation, with maximum values at $\Psi_{\text{N,S}} \approx 180^\circ$ for both systems, such that it points in the same direction as the field in the south lobe but opposite to the field in the north lobe, then the current sheet is displaced to the north. Clearly, the largest such effects will occur when the two systems are in phase during their beat cycle (at intervals of ~ 22 days), with the peak-to-peak amplitude for this specific data set under these conditions being found by *Provan et al.* [2012] to be $\sim 3 R_S$. Such displacements may thus be significant in relation to the displacement of the spacecraft from the current sheet (Figure 1e) and the consequent visibility of plasmoids/TCRs.

In addition to these effects, the PPOs also result in perturbations in the colatitudinal field component (B_θ , positive southward at the equator), which are in phase with the radial component for the southern system but in anti-phase with the radial component for the northern system. Thus, the southward field threading the equatorial plane is enhanced when $\Psi_{\text{N}} \approx 180^\circ$ and $\Psi_{\text{S}} \approx 0^\circ$ and weakened when $\Psi_{\text{N}} \approx 0^\circ$ and $\Psi_{\text{S}} \approx 180^\circ$. A likely related effect is seen in modulations in the thickness of the tail current sheet, which is thickened at phases when B_θ is enhanced and thinned when it is reduced. The largest such effects thus occur when the two systems are in antiphase during

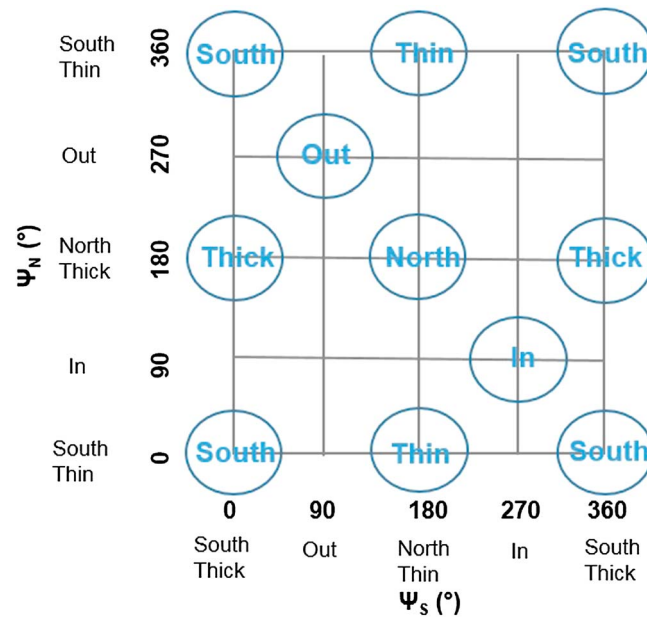


Figure 2. Schematic illustrating the expected perturbations of the tail current sheet depending on the joint phases of the northern (vertical) and southern (horizontal) PPO systems. The expected effects associated with each system alone are marked along the vertical and horizontal axes, where north and south refer to displacements of the current sheet away from the mean position, thick and thin refer to the total width of the current sheet associated with modulations of the B_r and B_θ field components, and out and in refer to radial displacements of the magnetospheric plasma and field lines (see section 3.1). The circled text within the grid then shows the phase combinations where both systems act in concert and thus where the largest such effects may be found. Southern phase effects are expected to be the larger of the two, by a factor of ~ 2 . With increasing time, the combined phase point (Ψ_S, Ψ_N) on this grid moves through 360° during each PPO period ~ 10.6 h for the northern PPO and 10.8 h for the southern PPO, thus tracing a line at an angle of slightly greater than 45° to the horizontal axis and rastering over the whole surface during each beat period of ~ 22 days.

systems act in concert during the beat cycle are indicated within the circles within the grid itself. As indicated above, the largest north-south displacements occur when both northern and southern systems are in phase along the central diagonal of the grid, while the largest variations in thickness occur at locations displaced by 180° on either side where they are in antiphase. During this interval the amplitude of the northern system was $\sim 40\%$ of that of the southern [Andrews et al., 2012], so that the southern system effects indicated along the horizontal axis are expected to be most important overall. However, the effect of the northern system may still be significant, increasing the overall effect to $\sim 140\%$ of the southern when they act in concert, and reducing it to $\sim 60\%$ of the southern when they act oppositely.

In addition to the north-south displacement and thickening-thinning effects discussed above, it has also been found that the magnetospheric plasma undergoes radial displacements during the PPO cycle as observed directly in the positions of the magnetopause [Clarke et al., 2010a] and bow shock [Clarke et al., 2010b], in the formation of the “plasma cam” effect [Burch et al., 2009], and in corresponding latitudinal displacements of the auroral field-aligned currents [Hunt et al., 2014]. For the southern system, maximum outward displacements occur at $\Psi_S \approx 90^\circ$ and inward displacements at $\Psi_S \approx 270^\circ$ as shown in Figure 2 (“out” and “in” along the horizontal axis), but while such displacements have not yet been demonstrated specifically for the northern system, the same physical considerations show that maximum outward displacements in this case should occur at $\Psi_N \approx 270^\circ$ and inward displacements at $\Psi_N \approx 90^\circ$ as shown along the vertical axis in Figure 2 [Hunt et al., 2015]. Plasmoid formation may then be expected to be enhanced when plasma mass is displaced outward by the PPO systems in the nightside sector, i.e., when $\Psi_S \approx 90^\circ$ and $\Psi_N \approx 270^\circ$. These combined conditions again

their beat cycle, under which condition Provan et al. [2012] found for this data set that the total current sheet width was $\sim 10 R_S$ when $\Psi_N \approx 180^\circ$ and $\Psi_S \approx 0^\circ$ (B_θ enhanced and B_r reduced in each lobe) but reduced to $\sim 4 R_S$ when $\Psi_N \approx 0^\circ$ and $\Psi_S \approx 180^\circ$ (B_θ reduced and B_r enhanced in each lobe). These effects may be expected to have a significant effect of the stability of the current sheet to reconnection. Stability is expected to be enhanced under the former of these conditions ($\Psi_N \approx 180^\circ$ and $\Psi_S \approx 0^\circ$) when lobe B_r is reduced and the current sheet widened, both reducing the cross-tail current density, and B_θ simultaneously enhanced, such that reconnection will then tend to be suppressed. However stability is expected to be reduced and reconnection favored under the latter conditions ($\Psi_N \approx 0^\circ$ and $\Psi_S \approx 180^\circ$) when lobe B_r is enhanced and the current sheet narrowed, both increasing the cross-tail current density, and B_θ simultaneously decreased.

These perturbations are indicated schematically in Figure 2, which shows a grid of northern phase Ψ_N plotted vertically versus southern phase Ψ_S plotted horizontally, with the above effects written at the corresponding phases as “north,” “south,” “thick,” and “thin” along the vertical and horizontal axes as appropriate. Joint phases at which the two

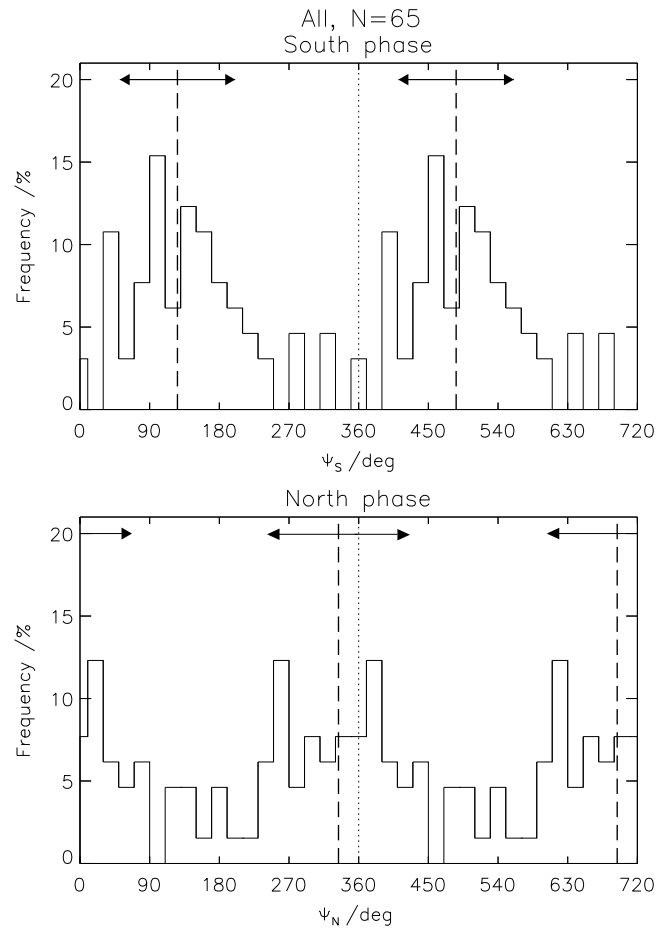


Figure 3. Histograms of plasmoid/TCR frequency versus (top) southern and (bottom) northern magnetic phase for all 65 grouped events, where two cycles of phase are plotted to aid visualization of the data modulation. Phases are calculated at the location of the inferred reconnection site, tracked back from the spacecraft location using equation (3) with radial phase propagation delay taken into account. The vertical dashed lines indicate the directional means of the data, while the horizontal arrowed lines indicate the circular standard deviations (see section 3.2).

occur when the two systems are in antiphase, in quadrature with the successive thickening and thinning cycle discussed above. Visibility effects aside, we may thus expect reconnection and plasmoids to occur preferentially as the combined phase point (Ψ_N, Ψ_S) on this grid, moving with time at an angle slightly greater than $\sim 45^\circ$ to the horizontal axis (northern period shorter than southern), and rastering over the whole surface during each beat cycle, traces in the vicinity of the adjacent regions marked out and “thin.”

3.2. Overall Plasmoid Dependence on Southern and Northern Phases

Taking this grouped data set of 65 events tailward of the X line, we now examine the occurrence of these events in relation to the PPO phases. Figure 3 shows occurrence histograms of these events as a function of southern phase (top panel) and northern phase (bottom panel) for all 65 events, where tracking to the inferred reconnection site and radial propagation delay has been taken into account as outlined in section 2.2. To aid visibility of the modulations, two cycles of phase are shown on the horizontal axis. In each plot the vertical dashed lines show the “directional mean” appropriate to these angular data, while the arrowed horizontal lines show the “circular standard deviation” about the mean. Following *Mardia and Jupp* [2000] (see also *Andrews et al.* [2011]), the directional mean of a set of K angles, θ_k , is given by

$$\theta' = \tan^{-1} \left(\frac{S'}{C'} \right), \tag{4}$$

where

$$S' = \frac{1}{K} \sum_{k=1}^K \sin(\theta_k) \text{ and } C' = \frac{1}{K} \sum_{k=1}^K \cos(\theta_k), \tag{5}$$

and the signs of the numerator and denominator in equation (4) are taken separately to define θ' over the full 360° range. The “mean resultant length” of the data, R' , is given by

$$R' = \sqrt{S'^2 + C'^2}, \tag{6}$$

from which the circular standard deviation (in radians) is given by

$$\sigma = \sqrt{\ln \left(\frac{1}{R'^2} \right)}. \tag{7}$$

Returning to Figure 3, we can see from the top panel that the majority of events clearly occur in the range of southern phase between $\sim 50^\circ$ and $\sim 200^\circ$ (modulo 360°), with a directional mean of 126° (vertical dashed line)

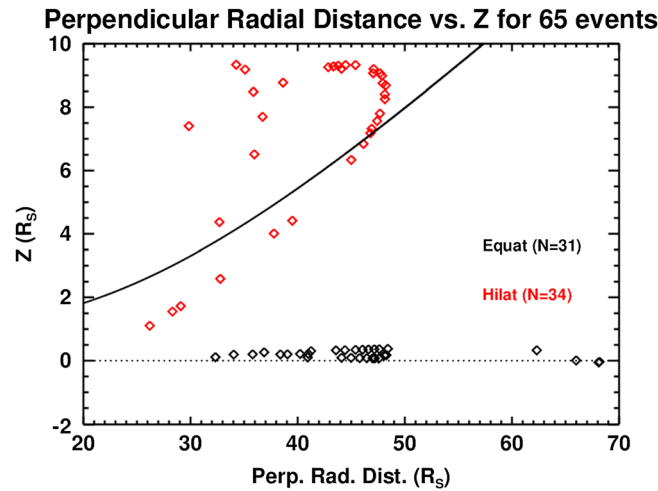


Figure 4. Plot of the spacecraft position in cylindrical coordinates for the 65 grouped plasmoids and TCRs, where z is positive northward from Saturn's equatorial plane and ρ is cylindrical distance from Saturn's spin/magnetic axis. The black diamonds show event positions observed on the initial equatorial orbits of the interval considered here with latitude less than 1° , while the red diamonds show event positions on the later high-latitude orbits. The solid black line shows the estimated mean position of the equatorial current sheet, $1 R_S$ northward of that given by the *Arridge et al.* [2008] model, calculated specifically for conditions in the middle of the year 2006 (days 142–162), though the variation over the interval is small.

outward (centered at $\Psi_S \approx 90^\circ$) and those for which the plasma sheet is thinned (colatitudinal field reduced centered at $\Psi_S \approx 180^\circ$), both conditions being conducive to tail reconnection and plasmoid release as discussed in section 3.1. Similarly, the distribution of northern phase, though broader, is also predominantly related to intervals in which the field lines are displaced outward and by sheet thinning. The stronger grouping by southern phase suggests that this effect is the stronger, as anticipated, but the similar clear grouping by northern phase indicates that these perturbations are also involved, such that the events occur preferentially during intervals when the two systems are near antiphase. This finding suggests that the phase effects are not linked strongly to visibility issues associated with north-south motions of the current sheet that maximize during in-phase intervals but are instead linked to the enhanced cycles of radial motion and plasma sheet field and thickness modulations that occur during antiphase intervals.

3.3. Separation of Equatorial and High-Latitude Events

As indicated in Figure 1, there are two distinct trajectory types in 2006, namely six initial orbits which explore Saturn's equatorial plane and latitudes within 1° of the equator, and three subsequent orbits which explore higher latitudes. The former category encompasses events up to \sim day 205 of 2006 when Cassini spent much of its time in the southern lobe, while the latter encompasses orbits after \sim day 205 when Cassini spent more time up near the average location of the hinged current sheet. The difference in nature of the equatorial and higher-latitude orbits is illustrated in Figure 4, which shows the location of the plasmoid and TCR events in cylindrical (ρ, z) coordinates, where black diamonds correspond to the equatorial orbits and red diamonds to the high-latitude orbits. The black curve shows the estimated mean position of the current sheet, $\sim 1 R_S$ northward of that indicated by the *Arridge et al.* [2008] model given by equation (1), recalling the results of *Provan et al.* [2012] mentioned in section 2 in relation to Figure 1e. It can be seen that the events on the equatorial orbits are typically observed several R_S south of the mean current sheet center, while those on the higher-latitude orbits are by virtue of the orbit observed closer to the mean position and both north and south of the sheet center. If event visibility were an issue with these data, we might expect the events on equatorial orbits to favor conditions when the current sheet is displaced southward toward the spacecraft and to disfavor conditions when it is displaced northward. That is, for the stronger southern system we might expect to retain events in the distribution in a broad sector of phase around $\Psi_S \approx 0^\circ$ where the current sheet is displaced southward (see Figure 2) and to lose events in a broad sector around $\Psi_S \approx 180^\circ$ where the current sheet is displaced northward.

and a circular standard deviation of 75° . Since maxima of the southern SKR occur when $\Psi_S \approx 180^\circ$ during this interval, these events usually correspond to southern phase at which the southern SKR is increasing toward a maximum, as found in the initial study of a small number of events by *Jackman et al.* [2009b]. Figure 3 (bottom) shows that the events are somewhat less organized by northern phase but have clear preference for phases between $\sim 230^\circ$ and $\sim 400^\circ$, with a directional mean of 334° and a standard deviation of 93° . Since northern SKR maxima correspondingly occur at northern phase $\Psi_N \approx 0^\circ/360^\circ$ during this interval, this range also generally corresponds to phases at which the northern SKR amplitude increases toward a maximum.

Referring to Figure 2, it can be seen that the range of southern phase for most of the events in the upper panel corresponds to those for which the magnetospheric plasma is displaced radially

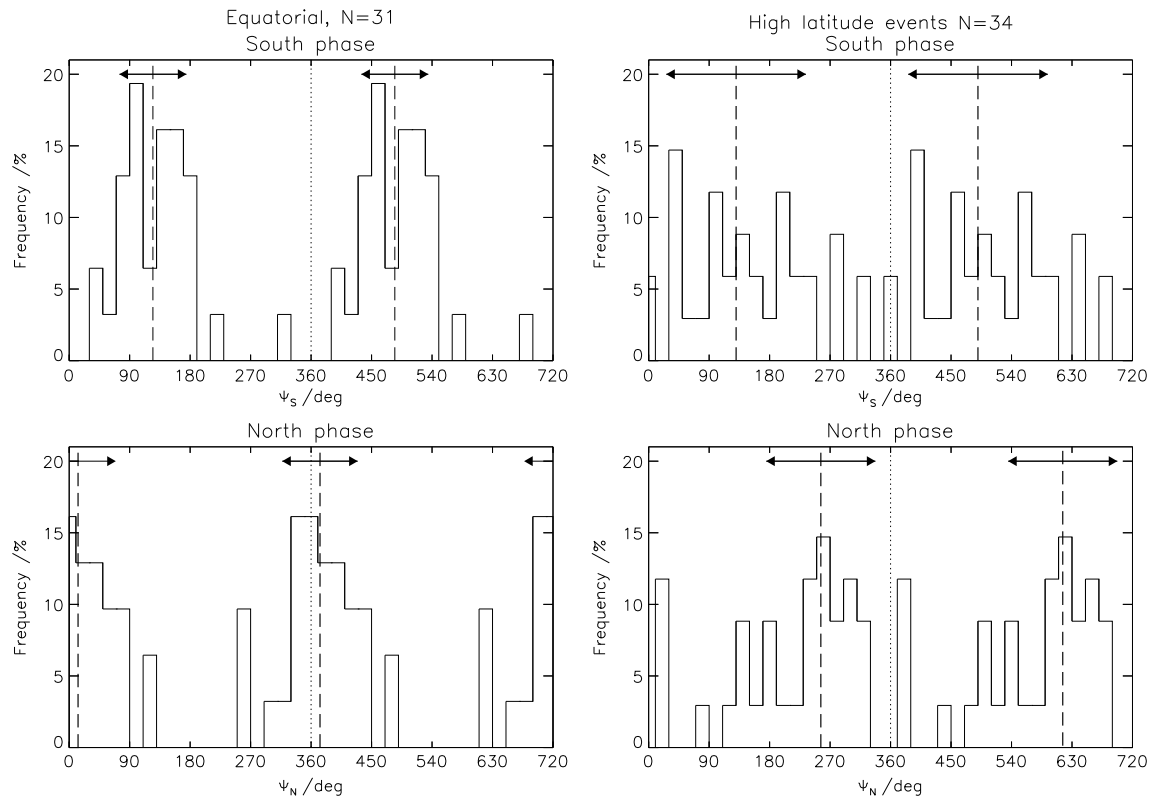


Figure 5. (a) Histograms of plasmoid/TCR occurrence frequency versus (top) southern and (bottom) northern phases for 31 events observed on equatorial orbits (latitude less than 1°), in the same format as Figure 3. (b) Histograms of plasmoid/TCR occurrence frequency versus southern (top) phase and northern (bottom) phase for 34 events observed on high-latitude orbits, in the same format as Figures 3 and 5a.

In Figure 5a we thus show histograms of occurrence frequency versus southern (top panel) and northern (bottom panel) phases for the 31 events observed near the equatorial plane in the same format as Figure 3. Contrary to the above expectation, we see that the distribution with respect to southern phase peaks at almost the same value as that of the whole distribution, at 125°, when the current sheet overall is expected to be displaced northward of the mean position (Figure 2), and is even more tightly grouped about that value with a circular standard deviation of 49°. This result thus continues to suggest an association with phases for which the field lines are displaced outward and the current sheet thinned (with enhanced lobe B_r and reduced B_θ) but again provides no indication that visibility is a major factor. Figure 5a (bottom) also shows a tighter grouping of the events versus northern phase, with a directional mean of 13° and a circular standard deviation of 56°. This range of phases again corresponds principally to thinning of the current sheet.

In Figure 5b we show results in the same format for the remaining 34 events observed nearer the mean position of the current sheet on the higher-latitude orbits. Here both distributions are considerably broader than for the equatorial events, suggesting a somewhat different population of reconnection-associated events compared with the equatorial orbits, perhaps distinguished by inclusion of events of smaller magnitude observed closer to the sheet center. We note again from Figure 1 that these events are considerably more numerous with time on the high-latitude orbits than on the equatorial. However, they are still somewhat ordered by southern and northern phases about similar values, with a directional mean of 130° and a circular standard deviation 104° for the southern phase distribution, and a directional mean of 256° and a circular standard deviation of 81° for the northern phase distribution. Both orderings in this case suggest a weaker association with outward displacement of the field lines and thinning of the current sheet.

3.4. Combined Influence of Northern and Southern Phases

Proceeding from the individual phase analyses shown in Figures 3 and 5, we now examine the phase dependencies jointly by plotting the event phases on the (Ψ_S , Ψ_N) plane as in Figure 2 and examining the event

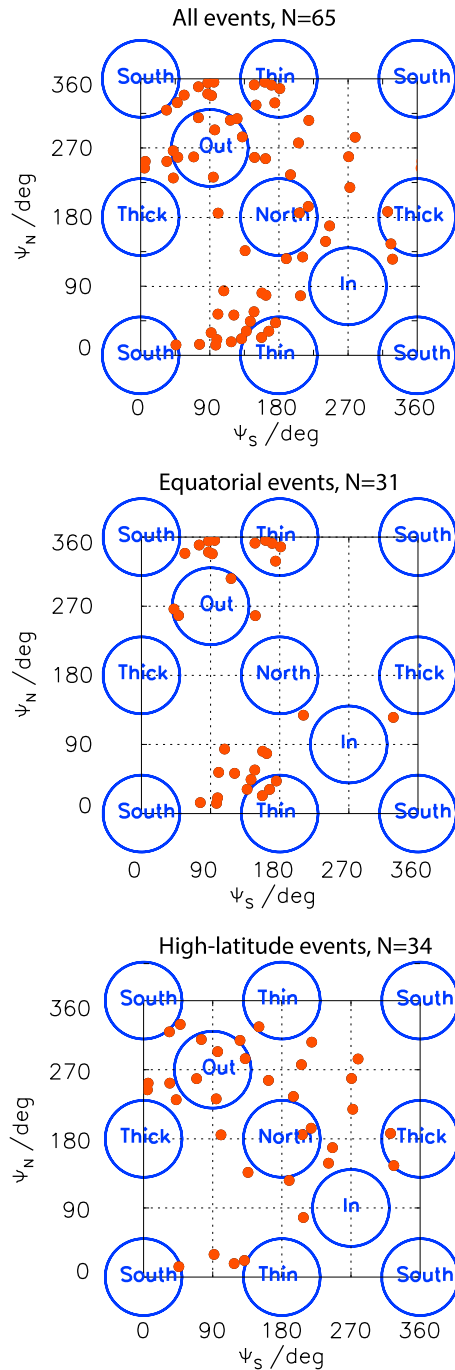


Figure 6. Scatterplots of plasmoid/TCR event occurrence on the southern-northern magnetic PPO phase plane, following the format of Figure 2. (top) All 65 events, (middle) 31 near-equatorial events, and (bottom) 34 high-latitude events.

occurrence relative to the expected current sheet perturbations indicated in the latter figure. Results are shown in Figure 6, where the top panel shows all 65 events (as in Figure 3), the middle panel the 31 events observed on the initial orbits close to Saturn’s equatorial plane (Figure 5a), and the bottom panel the 34 events observed on the higher-latitude orbits (Figure 5b). The tightest clustering of events, and thus the most evident degree of organization, is seen in Figure 6 (middle), for events observed near the equatorial plane. In this case, the occurrence of plasmoids/TCRs peaks in a distinct sector between southern phase $\sim 75^\circ\text{--}175^\circ$ and northern phase $\sim 70^\circ\text{--}300^\circ$. Comparing with the schematic in Figure 2, this region corresponds to conditions in which the magnetospheric field lines and plasma are displaced outward, particularly by the stronger southern system, and also in which the current sheet is thinned (with enhanced lobe B_r and reduced B_θ) due to both systems. These are conditions favorable to reconnection and plasmoid formation, as discussed in section 3.1. It is notable that there are almost no events at phases where the plasma and field lines are displaced inward, nor where the current sheet is thickened (with reduced lobe B_r and enhanced B_θ) during the PPO cycle. The events observed on high-latitude orbits (Figure 5b) typically closer to the mean position of the current sheet (Figure 4) are more broadly spread, again suggesting a somewhat different overall population to those observed near the planetary equator, but they again favor phases associated with outward displacements of the plasma and field, and thinned current sheet.

4. Summary and Conclusions

Here we have examined the relationship between reconnection-related plasmoid and TCR events observed in Saturn’s tail by the Cassini magnetometer, and the northern and southern magnetic phases of the PPO phenomenon, with an aim to understand the extent to which magnetotail dynamics at Saturn are governed by these periodicities. For this interval, however, due to the weaker northern magnetic system then prevailing ($\sim 40\%$ by amplitude of the southern), the northern SKR phase has been used as a direct proxy for the northern magnetic phase in this study. Previous work has shown that the tail current sheet is strongly modulated by the PPO phases, with maximal north-south oscillations occurring when the northern and southern magnetic systems are in phase, together with maximal thickening and thinning together with associated current sheet field perturbations when

they are in antiphase [Provan *et al.*, 2012]. In addition, it has been found that magnetospheric flux tubes and plasma are radially displaced during the PPO cycle [Burch *et al.*, 2009; Clarke *et al.*, 2010a, 2010b; Hunt *et al.*, 2014, 2015], with maximum effects also expected when the two systems are in antiphase, these modulations being in quadrature with the thickening and thinning cycle. In general, such perturbations may potentially modulate both the occurrence of reconnection and the visibility of the events formed thereby.

Overall, this study has shown a strong link between plasmoid/TCR event occurrence in these data and the phases of both the stronger southern and weaker northern systems. Specifically, the events preferentially occur for phases associated with outward displacement of the plasma, particularly for the stronger southern system, and for thinned current sheets with enhanced radial and reduced southward fields, both a priori likely to increase the likelihood of tail reconnection and plasmoid release taking place. These correspond to phases in which the SKR emission is rising toward a maximum for the stronger southern system, as found previously by *Jackman et al.* [2009b] for a much smaller data set, and to phases prior to and during SKR maximum for the weaker northern system. No clear signature was found indicating a major influence on event visibility due to north-south motions of the current sheet. The greatest degree of organization was found for events observed near Saturn's equatorial plane earlier in the interval examined, which may correspond to larger events observed typically several Saturn radii south of the current sheet center. The more temporally numerous events observed on high-latitude orbits typically closer to the center of the sheet, which may contain an additional population of smaller-scale events, are rather more scattered but still have a degree of organization at these same phases indicative of reconnection modulation by radial displacement of the plasma and current sheet thinning. Overall, these results thus clearly demonstrate that tail dynamics and plasmoid formation in Saturn's magnetosphere are strongly modulated by the PPO-associated field and plasma perturbations.

Appendix A

Table A1 shows details for the 65 reconnection events considered in this study.

Table A1. List of the Times of 65 "Grouped" Reconnection Events From the J14 Catalogue, Including Information on Their Location, Phase, and Position Relative to the Model Current Sheet

Range OBS (R_S)	Latitude (deg)	LT (h)	Range RCN (R_S)	South Phase RCN Radial Propagation (deg)	North Phase RCN Radial Propagation (deg)	ZCS_OBS_BOWL (R_S)	(ZSC – ZBOWL) OBS (R_S)
66.0	0.008	4.43	45.50	148.25	257.70	12.52	-12.51
68.2	-0.027	4.77	46.59	181.15	347.27	13.18	-13.21
68.1	-0.043	4.93	46.54	161.56	355.77	13.14	-13.19
32.3	0.203	2.28	28.67	116.67	306.06	2.93	-2.81
40.9	0.147	2.92	32.97	157.38	23.28	4.95	-4.85
44.1	0.123	3.17	34.55	92.17	338.21	5.78	-5.69
45.0	0.116	3.25	34.99	87.35	340.42	6.02	-5.93
45.8	0.108	3.33	35.39	95.31	355.76	6.24	-6.15
46.5	0.101	3.41	35.73	87.37	354.88	6.42	-6.34
47.0	0.094	3.48	36.00	75.17	349.65	6.57	-6.49
47.2	0.091	3.51	36.10	210.88	128.08	6.63	-6.55
47.6	0.085	3.57	36.30	157.82	81.17	6.74	-6.66
34.0	0.330	0.55	29.52	147.82	352.12	3.25	-3.05
35.8	0.323	0.12	30.40	48.35	257.90	3.64	-3.44
40.2	0.307	0.97	32.61	42.31	266.36	4.70	-4.48
40.9	0.304	1.01	32.95	175.61	42.40	4.87	-4.65
38.4	0.300	0.72	31.70	174.63	328.69	4.13	-3.93
39.1	0.297	0.75	32.03	327.93	125.22	4.28	-4.08
48.3	0.209	2.02	36.64	163.08	78.21	6.61	-6.43
48.1	0.204	2.08	36.55	99.16	20.50	6.56	-6.38
62.3	0.303	1.57	43.66	170.23	351.82	10.29	-9.96
48.4	0.446	23.86	36.71	166.81	31.45	6.34	-5.96
47.6	0.442	0.15	36.31	137.55	31.57	6.12	-5.75
47.2	0.441	0.22	36.08	142.66	44.29	6.00	-5.64
46.5	0.439	0.05	35.75	147.54	56.75	5.84	-5.48
46.1	0.438	0.37	35.53	97.75	13.41	5.72	-5.37
45.4	0.436	0.43	35.21	56.55	338.85	5.56	-5.21
44.4	0.434	0.53	34.71	121.30	52.42	5.31	-4.98
43.5	0.431	0.61	34.25	76.63	14.29	5.09	-4.76
41.3	0.425	0.80	33.13	100.54	53.68	4.55	-4.24
36.9	0.412	1.13	30.94	108.22	84.00	3.57	-3.30
36.9	13.313	22.40	30.93	94.55	232.03	3.53	4.96
43.9	12.189	22.93	34.43	150.17	325.84	5.11	4.14
44.3	12.088	22.97	34.67	325.83	145.17	5.23	4.06

Table A1. (continued)

Range OBS (R_S)	Latitude (deg)	LT (h)	Range RCN (R_S)	South Phase RCN Radial Propagation (deg)	North Phase RCN Radial Propagation (deg)	ZCS_OBS_BOWL (R_S)	(ZSC – ZBOWL) OBS (R_S)
44.8	11.997	23.01	34.88	125.50	308.18	5.33	3.97
45.4	11.841	23.10	35.20	42.44	230.90	5.49	3.84
46.4	11.609	23.16	35.70	96.40	293.54	5.73	3.60
48.0	11.053	23.37	36.50	34.07	252.48	6.12	3.08
48.5	10.763	23.48	36.75	208.04	77.55	6.24	2.82
48.7	10.638	23.52	36.85	75.16	309.39	6.29	2.70
49.0	10.208	23.67	37.00	131.27	21.60	6.36	2.32
48.9	9.731	23.83	36.93	240.75	148.28	6.32	1.94
48.3	9.294	23.98	36.66	245.98	168.53	6.18	1.62
47.5	8.871	0.11	36.24	189.52	125.83	5.97	1.35
38.0	6.059	0.94	31.50	279.22	283.98	3.73	0.28
30.8	13.936	21.91	27.88	132.32	284.41	2.28	5.12
39.6	12.788	22.56	32.30	69.01	258.34	4.05	4.72
45.0	11.797	22.99	35.00	321.49	187.11	5.28	3.93
47.9	10.910	23.33	36.45	117.88	17.61	5.98	3.09
48.7	10.347	23.53	36.87	47.64	329.00	6.17	2.58
48.8	9.910	23.68	36.90	91.72	29.47	6.19	2.22
48.0	9.066	23.91	36.51	45.93	13.56	5.99	1.58
47.3	8.727	0.02	36.15	206.63	185.40	5.81	1.38
46.6	8.437	0.15	35.82	270.75	258.59	5.64	1.20
45.5	8.013	0.27	35.23	135.93	136.28	5.35	0.98
39.7	6.380	0.75	32.37	195.05	235.09	4.04	0.38
32.8	4.518	1.26	28.90	205.49	276.57	2.62	−0.03
29.1	3.399	1.56	27.07	100.76	185.15	1.98	−0.25
28.4	3.144	1.63	26.68	218.91	305.86	1.85	−0.29
26.2	2.419	1.82	25.61	162.56	256.07	1.52	−0.42
35.4	15.240	23.92	30.20	4.91	243.82	3.10	6.24
36.2	14.669	0.02	30.60	5.88	252.51	3.26	5.93
37.5	11.839	0.52	31.26	33.61	319.31	3.52	4.18
36.5	10.270	0.77	30.77	272.36	218.49	3.31	3.20
33.0	7.617	1.21	29.00	218.14	193.81	2.62	1.75

Acknowledgments

C.M.J. is supported by a Science and Technology Facilities Council Ernest Rutherford Fellowship. Work at Leicester is supported by STFC consolidated grant ST/K001000/1. The SKR phases are available from the Cassini RPWS HFR data server [Lamy, 2008; <http://www.lesia.obspm.fr/kronos>], and C.M.J. acknowledges Laurent Lamy for these. C.M.J. acknowledges useful discussion with Chris Arridge. The magnetic field phases are available from G.P. C.M.J. thanks M.K. Dougherty for access to Cassini magnetometer data, and S. Kellock and L. Alconcel at Imperial College London for MAG data processing. Cassini MAG data processing activities are supported in the United Kingdom by STFC. Cassini MAG data used in this study may be obtained from the Planetary Data System (<http://pds.nasa.gov/>).

References

Andrews, D. J., E. J. Bunce, S. W. H. Cowley, M. K. Dougherty, G. Provan, and D. J. Southwood (2008), Planetary period oscillations in Saturn's magnetosphere: Phase relation of equatorial magnetic field oscillations and SKR modulation, *J. Geophys. Res.*, *113*, A09205, doi:10.1029/2007JA012937.

Andrews, D. J., A. J. Coates, S. W. H. Cowley, M. K. Dougherty, L. Lamy, G. Provan, and P. Zarka (2010), Magnetospheric period oscillations at Saturn: Comparison of equatorial and high-latitude magnetic field periods with north and south SKR periods, *J. Geophys. Res.*, *115*, A12252, doi:10.1029/2010JA015666.

Andrews, D. J., B. Cecconi, S. W. H. Cowley, M. K. Dougherty, L. Lamy, G. Provan, and P. Zarka (2011), Planetary period oscillations in Saturn's magnetosphere: Evidence in magnetic field phase data for rotational modulation of Saturn kilometric radiation emissions, *J. Geophys. Res.*, *116*, A09206, doi:10.1029/2011JA016636.

Andrews, D. J., S. W. H. Cowley, M. K. Dougherty, L. Lamy, G. Provan, and D. J. Southwood (2012), Planetary period oscillations in Saturn's magnetosphere: Evolution of magnetic oscillation properties from southern summer to postequinox, *J. Geophys. Res.*, *117*, A04224, doi:10.1029/2011JA017444.

Arridge, C. S., K. K. Khurana, C. T. Russell, D. J. Southwood, N. Achilleos, M. K. Dougherty, A. J. Coates, and H. K. Leinweber (2008), Warping of Saturn's magnetospheric and magnetotail current sheets, *J. Geophys. Res.*, *113*, A08217, doi:10.1029/2007JA012963.

Arridge, C. S., et al. (2011), Periodic motion of Saturn's nightside plasma sheet, *J. Geophys. Res.*, *116*, A11205, doi:10.1029/2011JA016827.

Arridge, C. S., et al. (2015), Cassini in situ observations of long duration magnetic reconnection in Saturn's magnetotail, *Nat. Phys.*, doi:10.1038/nphys3565.

Bunce, E. J., S. W. H. Cowley, D. M. Wright, A. J. Coates, M. K. Dougherty, N. Krupp, W. S. Kurth, and A. M. Rymer (2005), In situ observations of a solar wind compression-induced hot plasma injection in Saturn's tail, *Geophys. Res. Lett.*, *32*, L20504, doi:10.1029/2005GL022888.

Burch, J. L., J. Goldstein, P. Mokashi, W. S. Lewis, C. Paty, D. T. Young, A. J. Coates, M. K. Dougherty, and N. André (2008), On the cause of Saturn's plasma periodicity, *Geophys. Res. Lett.*, *35*, L14105, doi:10.1029/2008GL034951.

Burch, J. L., A. D. DeJong, J. Goldstein, and D. T. Young (2009), Periodicity in Saturn's magnetosphere: Plasma cam, *Geophys. Res. Lett.*, *36*, L14203, doi:10.1029/2009GL039043.

Carbary, J. F., and D. G. Mitchell (2013), Periodicities in Saturn's magnetosphere, *Rev. Geophys.*, *51*, 1–30, doi:10.1002/rog.20006.

Clarke, K. E., D. J. Andrews, C. S. Arridge, A. J. Coates, and S. W. H. Cowley (2010a), Magnetopause oscillations near the planetary period at Saturn: Occurrence, phase, and amplitude, *J. Geophys. Res.*, *115*, A08209, doi:10.1029/2009JA014745.

Clarke, K. E., D. J. Andrews, A. J. Coates, S. W. H. Cowley, and A. Masters (2010b), Magnetospheric period oscillations of Saturn's bow shock, *J. Geophys. Res.*, *115*, A05202, doi:10.1029/2009JA015164.

- Cowley, S. W. H., D. M. Wright, E. J. Bunce, A. C. Carter, M. K. Dougherty, G. Giampieri, J. D. Nichols, and T. R. Robinson (2006), Cassini observations of planetary-period magnetic field oscillations in Saturn's magnetosphere: Doppler shifts and phase motion, *Geophys. Res. Lett.*, *33*, L07104, doi:10.1029/2005GL025522.
- Dougherty, M. K., et al. (2004), The Cassini magnetic field investigation, *Space Sci. Rev.*, *114*, 331–383, doi:10.1007/s11214-004-1432-2.
- Giampieri, G., M. K. Dougherty, E. J. Smith, and C. T. Russell (2006), A regular rotation period for Saturn's magnetic field that may track its internal rotation, *Nature*, *441*, 62–64, doi:10.1038/nature04750.
- Gurnett, D. A., A. Lecacheux, W. S. Kurth, A. M. Persoon, J. B. Groene, L. Lamy, P. Zarka, and J. F. Carbary (2009), Discovery of a north-south asymmetry in Saturn's radio rotation period, *Geophys. Res. Lett.*, *36*, L16102, doi:10.1029/2009GL039621.
- Gurnett, D. A., J. B. Groene, T. F. Averkamp, W. S. Kurth, S.-Y. Ye, and G. Fischer (2011), The SLS4 longitude system based on a tracking filter analysis of the rotational modulation of Saturn kilometric radiation, in *Planetary Radio Emissions VII*, pp. 51–64, Austrian Acad. Sci., Vienna.
- Hill, T. W., et al. (2008), Plasmoids in Saturn's magnetotail, *J. Geophys. Res.*, *113*, A01214, doi:10.1029/2007JA012626.
- Hunt, G. J., S. W. H. Cowley, G. Provan, E. J. Bunce, I. I. Alexeev, E. S. Belenkaya, V. V. Kalegaev, M. K. Dougherty, and A. J. Coates (2014), Field-aligned currents in Saturn's southern nightside magnetosphere: Subcorotation and planetary period oscillation components, *J. Geophys. Res. Space Physics*, *119*, 9847–9899, doi:10.1002/2014JA020506.
- Hunt, G. J., S. W. H. Cowley, G. Provan, E. J. Bunce, I. I. Alexeev, E. S. Belenkaya, V. V. Kalegaev, M. K. Dougherty, and A. J. Coates (2015), Field-aligned currents in Saturn's northern nightside magnetosphere: Evidence for inter-hemispheric current flow associated with planetary period oscillations, *J. Geophys. Res. Space Physics*, *120*, 7552–7584, doi:10.1002/2015JA021454.
- Jackman, C. M., and C. S. Arridge (2011), Statistical properties of the magnetic field in the kronian magnetotail lobes and current sheet, *J. Geophys. Res.*, *116*, A05224, doi:10.1029/2010JA015973.
- Jackman, C. M., C. T. Russell, D. J. Southwood, C. S. Arridge, N. Achilleos, and M. K. Dougherty (2007), Strong rapid dipolarizations in Saturn's magnetotail: In situ evidence of reconnection, *Geophys. Res. Lett.*, *34*, L11203, doi:10.1029/2007GL029764.
- Jackman, C. M., et al. (2008), A multi-instrument view of tail reconnection at Saturn, *J. Geophys. Res.*, *113*, A11213, doi:10.1029/2008JA013592.
- Jackman, C. M., C. S. Arridge, H. J. McAndrews, M. G. Henderson, and R. J. Wilson (2009a), Northward field excursions in Saturn's magnetotail and their relationship to magnetospheric periodicities, *Geophys. Res. Lett.*, *36*, L16101, doi:10.1029/2009GL039149.
- Jackman, C. M., L. Lamy, M. P. Freeman, P. Zarka, B. Cecconi, W. S. Kurth, S. W. H. Cowley, and M. K. Dougherty (2009b), On the character and distribution of lower-frequency radio emissions at Saturn and their relationship to substorm-like events, *J. Geophys. Res.*, *114*, A08211, doi:10.1029/2008JA013997.
- Jackman, C. M., J. A. Slavin, and S. W. H. Cowley (2011), Cassini observations of plasmoid structure and dynamics: Implications for the role of magnetic reconnection in magnetospheric circulation at Saturn, *J. Geophys. Res.*, *116*, A10212, doi:10.1029/2011JA016682.
- Jackman, C. M., N. Achilleos, S. W. H. Cowley, E. J. Bunce, A. Radioti, D. Grodent, S. V. Badman, M. K. Dougherty, and W. Pryor (2013), Auroral counterpart of magnetic field dipolarizations in Saturn's tail, *Planet. Space Sci.*, *82–83*, 34–42, doi:10.1016/j.pss.2013.03.010.
- Jackman, C. M., et al. (2014), Saturn's dynamic magnetotail: A comprehensive magnetic field and plasma survey of plasmoids and traveling compression regions and their role in global magnetospheric dynamics, *J. Geophys. Res. Space Physics*, *119*, 5465–5494, doi:10.1002/2013JA019388.
- Jackman, C. M., et al. (2015), Field dipolarization in Saturn's magnetotail with planetward ion flows and energetic particle flow bursts: Evidence of quasi-steady reconnection, *J. Geophys. Res. Space Physics*, *120*, 3603–3617, doi:10.1002/2015JA020995.
- Jia, X., K. C. Hansen, T. I. Gombosi, M. G. Kivelson, G. Tóth, D. L. DeZeeuw, and A. J. Ridley (2012), Magnetospheric configuration and dynamics of Saturn's magnetosphere: A global MHD simulation, *J. Geophys. Res.*, *117*, A05225, doi:10.1029/2012JA017575.
- Kurth, W. S., T. F. Averkamp, D. A. Gurnett, J. B. Groene, and A. Lecacheux (2008), An update to a Saturnian longitude system based on kilometric radio emissions, *J. Geophys. Res.*, *113*, A05222, doi:10.1029/2007JA012861.
- Lamy, L. (2011), Variability of southern and northern SKR periodicities, in *Planetary Radio Emissions VII*, edited by H. O. Rucker et al., pp. 39–50, Austrian Acad. of Sci. Press, Vienna.
- Mardia, K. V., and P. E. Jupp (2000), *Directional Statistics*, Wiley, Chichester, U. K.
- Mitchell, D. G., et al. (2005), Energetic ion acceleration in Saturn's magnetotail: Substorms at Saturn? *Geophys. Res. Lett.*, *32*, L20501, doi:10.1029/2005GL022647.
- Provan, G., D. J. Andrews, C. S. Arridge, S. W. H. Cowley, S. E. Milan, M. K. Dougherty, and D. M. Wright (2009), Polarization and phase of planetary-period magnetic field oscillations on high latitude field lines in Saturn's magnetosphere, *J. Geophys. Res.*, *114*, A02225, doi:10.1029/2008JA013782.
- Provan, G., D. J. Andrews, B. Cecconi, S. W. H. Cowley, M. K. Dougherty, L. Lamy, and P. Zarka (2011), Magnetospheric period magnetic field oscillations at Saturn: Equatorial phase "jitter" produced by superposition of southern- and northern-period oscillations, *J. Geophys. Res.*, *116*, A04225, doi:10.1029/2010JA016213.
- Provan, G., D. J. Andrews, C. S. Arridge, A. J. Coates, S. W. H. Cowley, G. Cox, M. K. Dougherty, and C. M. Jackman (2012), Dual periodicities in planetary-period magnetic field oscillations in Saturn's tail, *J. Geophys. Res.*, *117*, A01209, doi:10.1029/2011JA017104.
- Russell, C. T., C. M. Jackman, H. Y. Wei, C. Bertucci, and M. K. Dougherty (2008), Titan's influence on Saturnian substorm occurrence, *Geophys. Res. Lett.*, *35*, L12105, doi:10.1029/2008GL034080.
- Slavin, J., E. Smith, B. Tsurutani, D. Sibeck, H. Singer, D. Baker, J. Gosling, E. Hones, and F. Scarf (1984), Substorm-associated traveling compression regions in the distant tail: ISEE-3 geotail observations, *Geophys. Res. Lett.*, *11*, 657–660, doi:10.1029/GL011i007p00657.
- Thomsen, M. F., R. J. Wilson, R. L. Tokar, D. B. Reisenfeld, and C. M. Jackman (2013), Cassini/CAPS observations of duskside tail dynamics at Saturn, *J. Geophys. Res. Space Physics*, *118*, 5767–5781, doi:10.1002/jgra.50552.